Characterization of Quantum Dynamically Significant Paths of Bridge-Mediated Charge Transfer Systems

Eunji Sim* and Heeyoung Kim

Department of Chemistry, Yonsei University, 134 Sinchondong Seodaemungu, Seoul 120-749, Korea

Received: November 22, 2005; In Final Form: March 20, 2006

In this article, we examine characteristics of quantum dynamically important paths using the on-the-fly filtered propagator functional path integral method, which evaluates a numerically accurate reduced density matrix by ignoring the vast majority of paths with insignificant contribution to the dynamics of interest. Two five-state charge-transfer systems have been considered, such that each system is governed by a different charge-transfer mechanism. It was found that, for the incoherent hopping transfer, the quantum mechanically important paths mimic classical counterparts that show little deviation between forward and backward path. Therefore, it is desirable to take advantage of *a priori* knowledge of the important path characteristics; in particular, it is possible to evaluate the accurate dynamics of bridge-mediated long-range charge-transfer systems efficiently in a significantly reduced quantum mechanical trajectory space.

1. Introduction

Fundamental postulates of quantum mechanics stipulate that a quantum mechanical state be fully expressed in terms of a wave function or a density matrix of a chosen discrete representation. Any physical observation including time-dependent dynamical measurements can be deduced out of the time evolution of the wave function or density matrixes. In classical mechanics, for a given boundary condition, finding the classical path has a definite solution because there is only one allowed path. In quantum mechanics, however, infinite numbers of paths are diffused in the time-position space, that is, trajectory space, even for a one-dimensional problem. Furthermore, for many-body systems including condensed phase, it is a formidable task to evaluate density matrixes in full dimensions because the amount of calculations increases exponentially with the dimensionality of the system. Various schemes have been developed in order to overcome such limitations, some of which have shown significant improvement in efficiency and proven to be useful in predicting quantum dynamics in complex systems.[1]

An alternative way of reducing the amount of the computation with increasing dimensionality is the use of the system-bath Hamiltonian that separates the total system into a subsystem, which is directly involved in the process of interest, and the rest of the system whose presence indirectly influences the dynamics of the subsystem. The dynamics of the subsystem is obtained as the form of the reduced density matrix that is defined as

$$\tilde{\rho}(t) = Tr_b[e^{-iHt/\hbar}\rho(0)e^{iHt/\hbar}] \quad (1)$$

where taking the trace with respect to all bath degrees of freedom is denoted as Tr_b. The reduced density matrix, then, can be rewritten as a product of the bare system dynamics in the absence of the bath and the influence functional that describes the environmental effect on the system dynamics. Feynman's path integral approach is one of the most promising methodologies to provide an accurate description of the quantum dynamics.[2,3] Recent applications of path integral approaches have been successful on various phenomena in condensed phase ranging from atom−laser interaction[4] to transport such as diffusion,[5] coherence,[6] and electron dynamics[7,8] of the complex systems. Nevertheless, non-Markovian property of the influence functional, which arises from removal of the bath degrees of freedom, gives rise to a nonlocal memory function in time. Even for a one-dimensional M state system, the total number of discretized paths increases as $(M^2)^{N+1}$ where N is the number of discretized points in time.

Interesting quantum dynamical problems often involve a large number of states. In particular, elucidation of the charge transfer (CT) mechanism with respect to the bridge length has drawn tremendous interest in recent years along with the effort to develop an efficient molecular wire system that can conduct charges on the molecular level. Both experimentally and theoretically, determination of the CT mechanism has been conducted through the detection of the charge accumulation on each local site and through the distance and temperature dependence of the overall transfer rate constants. The CT kinetics is a complicated function of potential parameters wherein donor (acceptor) populations no longer exhibit simple single exponential decays (rises), especially when bridges between the donor and acceptor states are actively involved in the transfer dynamics, the so called incoherent hopping mechanism. Although the transfer mechanism should be determined by dynamical aspects, conventional approaches use steady-state transfer rates where the bridge population no longer changes rapidly in time. In the limit of the incoherent hopping, the transfer rate constant follows Ohm's law with respect to the donor−acceptor distance (R_{DA}) as $k \propto 1/R_{DA}$, while that of the coherent superexchange mechanism is rather insensitive to the distance change as $k \propto \exp(-\beta R_{DA})$ with inverse decay length β generally depending on energies.[9] In recent publications, it has been discussed that a potential intermediate transfer mechanism, called the partially coherent hopping mechanism, exists and rate constants of the partially coherent hopping-dominated

* Corresponding author. E-mail: esim@yonsei.ac.kr. Fax: +82-2-364-7050.

10.1021/jp056763w CCC: $33.50 © 2006 American Chemical Society
Published on Web 06/17/2006

CT process have shown excellent agreement with those from the McConnell's effective two-state system.[8,10] In general, the effective two-state system models coherent superexchange processes ignoring virtual bridges that merely mediate donor and acceptor without populating charges. Therefore, detailed dynamics through all of the possible pathways is required for an accurate description of the mechanism of the long-range CT processes.

Reduced density matrix evaluation in eq 1 relies on the efficient path integration scheme over a huge trajectory space whose size grows exponentially with propagation time as well as with the size of the system, that is, the number of electronic states. A conventional approach for huge space integration is to use a statistical means, such as path-integral Monte Carlo samplings. Although it has provided vital insights and accurate description for various imaginary-time path integrations, use of the statistical sampling for the real-time path integration has not been as successful because of the sign problem caused by oscillatory nature of the real-time propagators.[11] For the past decade, the real-time path integration methodologies have been improved rapidly by systematically reducing the number of paths to be summed without losing numerical accuracy. Egger and Mak have developed a path-integral Monte Carlo scheme with a filter technique that is optimized for dissipative spin systems employing the influence functional.[12,13] However, for exact integrations, Makarov and Makri first utilized the finite length of the bath memory to generalized Langevin-like dynamics simulations.[14,15] Later, further development was achieved by Sim and Makri, illustrating that, even for a quantum dynamics, not all of the paths are equally contributing.[16,17] The recently developed on-the-fly filtered propagator functional path integral (OFPF-PI) method successfully filters out the vast majority of less contributing paths without employing statistical methods.[18,19] The OFPF-PI has proven to be the most optimized in order to provide an accurate density matrix for the fairly long-time dynamics of large systems. Although it uses a smart filtering algorithm, the OFPF-PI, in principle, searches all of the possible trajectories in Hilbert space to select quantum dynamically important paths; thus, the size of the trajectory space is critical to the computational efficiency. For that reason, the long-range CT problem provides great challenge even for the most optimized OFPF-PI methodology because the number of electronic states exceeds three.

In this article, through the analysis of representative characteristics of quantum dynamically important paths, we aim to reduce the size of the trajectory space a priori. The article is organized as follows: in Section 2, we discuss the OFPF-PI formalism in which the reduced density matrix of the system coupled to a dissipative environment is obtained iteratively. Section 3 is devoted to the characterization of quantum dynamically important paths and to application to five-state long-range CT systems. Concluding remarks appear in Section 4.

2. On-the-Fly Filtered Propagator Functional Path Integral Method

For the long-range CT dynamics, it is advantageous to express the reduced density matrix in the locally excited single exciton representation rather than continuous coordinate representations. Supposing an M local state representation, the system Hamiltonian takes the form

$$H_s = \sum_{d=1}^{M} E_d |d\rangle\langle d| + \sum_{d=1}^{M}\sum_{d\neq d'}^{M} V_{dd'} |d\rangle\langle d'| \tag{2}$$

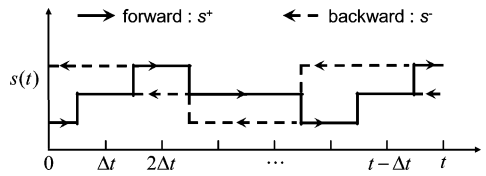

Figure 1. Typical forward and backward quantum mechanical path in time. The forward path (solid line) propagates from time zero to t, and the backward path (dashed line) propagates from t to zero.

Here, $|d\rangle$ describes the dth local single exciton state centered at $\tilde{s}_d$ and has the following relationship with the system coordinate operator:[20]

$$\langle d|\hat{s}|d'\rangle = \tilde{s}_d \delta_{dd'} \tag{3}$$

For the sake of simplicity, suppose the donor has the index of 1, that is, $|1\rangle$, and the acceptor corresponds to the index of M, that is, $|M\rangle$. The bridges are indexed consecutively such that they are denoted as $|2\rangle$ to $|M-1\rangle$. The system and the harmonic bath are assumed to have a bilinear form of interaction, and the damping strength of the bath is represented in terms of a spectral density instead of explicit coupling constants. The spectral density is obtained by spectral analysis of the force correlation functions.[21]

Owing to the use of local state representation and the time discretization of paths, Feynman and Vernon's influence functional formalism[2] simplifies eq 1 to a matrix multiplication form:

$$\tilde{\rho}(t) = \sum_{j}^{L_{tot}} \mathbf{S}(\Gamma_j^{(N)};\Delta t)\cdot\mathbf{F}(\Gamma_j^{(N)};\Delta t) \tag{4}$$

where $\tilde{\rho}$, $\mathbf{S}$, and $\mathbf{F}$ are $M \times M$ matrixes. The summation in eq 4 runs over all possible forward and backward paths (FB paths) connecting donor, bridges, and acceptor electronic states leading to exponential scale of $L_{tot} = M^{2N}$. In particular, the system propagator, $\mathbf{S}$, and the influence functional, $\mathbf{F}$, depend on $\Gamma_j^{(N)}$, which is the jth path segment among L_{tot} possible forward−backward trajectories that includes N forward time points from 0 to $t - \Delta t$ and additional N backward time points from $t - \Delta t$ to 0. A typical example of discretized FB path is illustrated in Figure 1. The system propagator in eq 4 is defined as

$$\mathbf{S}(\Gamma^{(N)};\Delta t) = \langle d_N^+|e^{-iH_s\Delta t/\hbar}|d_{N-1}^+\rangle \cdots \langle d_1^+|e^{-iH_s\Delta t/\hbar}|d_0^+\rangle\langle d_0^+|\tilde{\rho}(0)|d_0^-\rangle\langle d_0^-|e^{iH_s\Delta t/\hbar}|d_1^-\rangle \cdots \langle d_{N-1}^-|e^{iH_s\Delta t/\hbar}|d_N^-\rangle \tag{5}$$

where $|d_k^{\pm}\rangle$ denotes the local state at time $k\Delta t$ in the forward (+) and backward (−) direction of the $\Gamma^{(N)}$ path. The system propagator describes bare system dynamics in the absence of the bath. However, the influence of the bath fluctuation on the system dynamics is included in the influence functional as the following form:

$$\mathbf{F}(\Gamma^{(N)};\Delta t) = \exp\left(-\frac{1}{\hbar}\sum_{k=0}^{N}\sum_{k'=0}^{k}[\tilde{s}_k^+ - \tilde{s}_k^-][\eta_{kk'}.\tilde{s}_{k'}^+ - \eta_{kk'}^*\tilde{s}_{k'}^-]\right) \tag{6}$$

Expressions for the influence coefficients $\eta_{kk'}$ can be found elsewhere.[17] Owing to the influence coefficients arising from the nonlocal bath memory, the system exhibits non-Markovian dynamics that prevents iterative evaluation of eq 4. Because of the interference between bath modes, however, the bath response function $\alpha(t_1,t_2)$ and its discretized analogue $\eta_{kk'}$ decrease with $|t_1 - t_2|$ and $|k - k'|$, respectively. The OFPF-PI method takes

advantage of the fact that the nonlocal memory of the bath response function has a finite size in time so that the interaction is no longer present between the time points that are separated more than certain duration of time, say N_τ propagation time steps. Furthermore, it has been shown that, in general, the vast majority of quantum mechanical paths provide insignificant contribution to the dynamics and that they can be omitted without causing loss in numerical accuracy.[16] In practice, the OFPF-PI method performs full memory integration up to the bath memory and uses the approximate formulations for propagations at $t > \tau_m$ [18]

$$\tilde{\boldsymbol{\rho}}(t) = \sum_{w_j > \theta}^{L(t)} \mathbf{S}(\Gamma_j;\Delta t)\cdot\mathbf{F}(\Gamma_j;\Delta t), \quad N \le N_\tau \tag{7}$$

$$\tilde{\boldsymbol{\rho}}(t) \approx \sum_{w'_j > \theta}^{L(t)} \mathbf{S}(\Gamma'_j;\Delta t)\cdot\mathbf{F}(\Gamma'_j;\Delta t), \quad N > N_\tau \tag{8}$$

The summations in eqs 7 and 8 include only the paths with corresponding weight bigger than a predetermined weight cutoff, θ:

$$w_j = |\mathbf{S}(\Gamma_j;\Delta t)\cdot\mathbf{F}(\Gamma_j;\Delta t)|, \quad N \le N_\tau \tag{9}$$

$$w'_j = |\mathbf{S}(\Gamma'_j;\Delta t)\cdot\mathbf{F}(\Gamma'_j;\Delta t)|, \quad N > N_\tau \tag{10}$$

Note that the notation Γ'_j denotes the path segment with significant memory interaction within time points such that $\Gamma'_j = \{s^{\pm}_{N-N_\tau}, \cdots, s^{\pm}_{N-1}\}$. The weight cutoff is adjusted to provide desired numerical accuracy and is typically on the order of 10^{-8} to 10^{-10}.

Transfer probability through a particular pathway should be available in order to determine the transfer mechanism of complex systems. In other words, a quantitatively accurate partial density matrix of an individual transfer mechanism is needed. Recently, we have introduced a path integral formalism in which the reduced density matrix is decomposed into four partial density matrixes such that[19]

$$\tilde{\boldsymbol{\rho}}(t) = \tilde{\boldsymbol{\rho}}^{\mathbf{i}}(t) + \tilde{\boldsymbol{\rho}}^{\mathbf{c}}(t) + \tilde{\boldsymbol{\rho}}^{\mathbf{p}}(t) + \tilde{\boldsymbol{\rho}}^{\mathbf{s}}(t) \tag{11}$$

where $\tilde{\boldsymbol{\rho}}^{\mathbf{i}}(t)$ corresponds to incoherent hopping, $\tilde{\boldsymbol{\rho}}^{c}(t)$ corresponds to coherent superexchange, $\tilde{\boldsymbol{\rho}}^{p}(t)$ corresponds to partially coherent hopping, and $\tilde{\boldsymbol{\rho}}^{s}(t)$ corresponds to static mechanism. Although the static mechanism does not contribute to the transfer, inclusion of the static pathway is important for the path generation. It is clearly seen in eq 11 that each mechanism contributes to the full density matrix elements and is uncorrelated with the other, allowing independent computation of the partial density matrixes. Individual partial density matrix is calculated as eqs 7 and 8 except that the summation runs only over the pathways that belong to the corresponding mechanism.

3. Characteristics of Quantum Dynamically Important Paths

In this section, we explore the characteristics of quantum dynamically important paths for multistate CT systems embedded in a fluctuating medium. As depicted in Figure 2, we have chosen a system that consists of five diabatic surfaces of a donor, an acceptor, and three bridge states. Five-state CT systems are relatively less understood compared to the donor−bridge−acceptor triads; however, the dynamical behavior is diverse with respect to the energies and the couplings of the three bridge states. For instance, recent experiments on the electronic conductance in DNA performed by Giese et al. show that the CT mechanism varies depending on the bridge sequence.[22] By comparing transfer rate constants of 5′-G(AAA)GGG-3′ and 5′-G(AGA)GGG-3′ sequences, they speculate that, owing to the stable redox potential of the G/C nucleotide, charges hop to distant G/C base pairs by tunneling though A/T base pairs in between. The governing CT mechanism depends strongly on the choice of parameters that describe the system. Generally, it is difficult to predict the mechanism by a simple rule. Furthermore, few studies of various CT mechanisms have been conducted to date based on the quantitative analysis of CT pathways. In this article, to elucidate characteristics of CT mechanisms, we consider two sets of configurations and perform quantitative analysis on the quantum mechanical pathways that govern the corresponding CT processes. As drawn schematically in Figure 2, the energy differences are ΔE_{DB} (ΔE_{DA}) denoting that of donor and bridge (acceptor), while donor (acceptor) and the neighboring bridge interact with the strength of V_{DB} (V_{BA}). We assumed that the three bridge states have the same energy and the coupling between bridges is equal to V_{BB}. Potential parameters to describe the two five-state CT systems are listed in Table 1. The initial state is prepared so that only the donor is occupied and the rest of the system is unoccupied. Interaction between the system and the thermally equilibrated bath is turned on at time zero and the time evolution of the system population is evaluated.

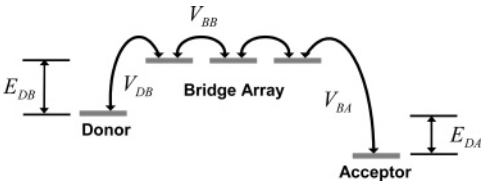

Figure 2. Schematic configuration of a five-state charge-transfer system with constant bridge energy. Energy differences and electronic coupling constants between states are summarized in Table 1.

TABLE 1: Potential Parameters for the Charge-Transfer Systems[a]

configuration	ΔE_{DB}	ΔE_{DA}	dV_{DB}	V_{BB}	V_{BA}	λ_{BA}	ω_c
F1	500	−900	22	50	135	900	600
F2	3790	−775	202	202	202	800	1700

[a] Units are in cm^{-1}.

A. Incoherent Hopping-Dominated Charge Transfer. First, we consider the CT system with the F1 configuration in Table 1. To represent the influence of the environment on the system dynamics, an ohmic form of the spectral density was chosen in which the reorganization energy provides an activationless transfer between the acceptor and the nearest-neighbor bridge. On the basis of the OFPF-PI formalism, the governing transfer mechanism can be determined through density matrix decomposition. In Figure 3, we compared the time evolution of the diagonal matrix elements ($\tilde{\rho}_{11}$ for the donor, $\tilde{\rho}_{22}$ to $\tilde{\rho}_{44}$ for the bridges, and $\tilde{\rho}_{55}$ for the acceptor) of the full path integration and those of the incoherent hopping pathway integration. The two integration results are indistinguishable and clearly show that the F1 configuration exhibits incoherent hopping CT. The overall transfer process begins with rapid CT from the donor to the nearest bridge state, then consecutive sequential transfer between bridge states is observed. Upon reaching the steady state, overall transfer between donor and acceptor is visible and the bridge population is almost constant for all bridges. Elucidation of the characteristics of pathways that mostly contribute to the incoherent hopping-dominated process is

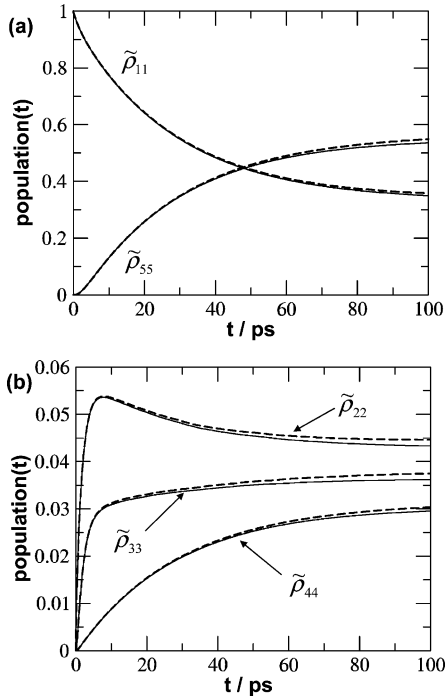

Figure 3. Five diagonal elements of reduced density matrix for the F1 configuration in Table 1; (a) donor ($\tilde{\rho}_{11}$) and acceptor ($\tilde{\rho}_{55}$) populations and (b) bridge ($\tilde{\rho}_{22}$, $\tilde{\rho}_{33}$, $\tilde{\rho}_{44}$) populations. Full path integration (solid lines) and incoherent hopping pathway integration (dashed lines) are indistinguishable. For all of the simulations shown, $\theta = 10^{-8}$ was used.

particularly interesting: It has been found that as the bridge length increases the incoherent hopping tends to dominate the transfer because of the exponential decrease of the superexchange coupling with the donor−acceptor distance.

Because the influence coefficients $\eta_{kk'}$ in eq 6 are complex numbers, we can rewrite $\eta_{kk'}$ as a sum of real and imaginary parts as $\eta_{kk'} = \epsilon_{kk'} + i\varphi_{kk'}$ with $\epsilon_{kk'}$ and $\varphi_{kk'}$ being real numbers. The influence functional of eq 6 then becomes a product of exponentials, respectively, with real and imaginary exponents as $\mathbf{F} = \mathbf{R}\cdot\mathbf{I}$:

$$\mathbf{R} = \exp\left(-\sum_{k=0}^{N}\sum_{k'=0}^{k}\frac{\epsilon_{kk'}}{\hbar}\Delta_k\Delta_{k'}\right) \tag{12}$$

$$\mathbf{I} = \exp\left(-i\sum_{k=0}^{N}\sum_{k'=0}^{k}\frac{\varphi_{kk'}}{\hbar}\Delta_k[\Delta_{k'} + 2\tilde{s}_{k'}^{-}]\right) \tag{13}$$

Here we substituted $\Delta_k = \Delta(k\Delta t) = \tilde{s}_k^{+} - \tilde{s}_k^{-}$, which denotes the difference between the forward path and backward path at time $k\Delta t$. Clearly, imaginary exponents in eq 13 give rise to cosine and sine functions; thus, it does not alter the magnitude of the influence functional. According to the expression in eq 12, the magnitude of the influence functional is large if $\Delta_k\Delta_{k'} \leq 0$ for all k and k'. Nevertheless, because the double summation adds $(N + 3)N/2 + 1$ terms and Δ_k can have either a positive or a negative sign, sums of $\Delta_k\Delta_{k'}$ cancel each other rapidly. Therefore, it is feasible to assume that the influence functional reaches its maximum where the forward path and corresponding backward path collapse at all times, that is, $\Delta_k = 0$, $k = 0$, ..., N. This is indeed the case for classical paths where the transfer process is completely incoherent. For quantum mechanical paths, however, it is well-known that no such constraint is applicable and the FB path segments are uncorrelated such that a CT system in vacuum will have a completely coherent dynamics without quantum decoherence introduced by baths. However, in the limit of the infinitely large system size, Imparato et al. have shown that the path integral is dominated by the classical paths.[23]

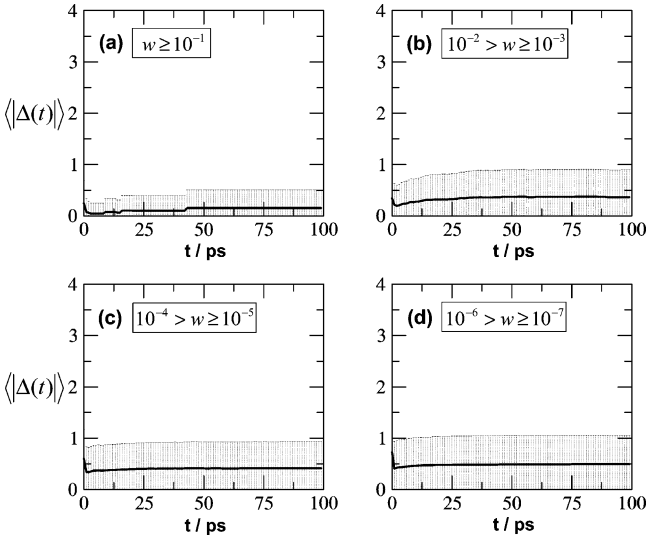

Figure 4. Average of the absolute difference between the forward and backward paths $|\Delta(t)| = |s^{+}(t) - s^{-}(t)|$ (solid line) and its standard deviation, $\sigma(t)$ (error bars) at room temperature for the F1 configuration in Table 1. The averages and corresponding standard deviations were taken from the paths with a weight as large as (a) $w \geq 10^{-1}$, (b) $10^{-2} > w \geq 10^{-3}$, (c) $10^{-4} > w \geq 10^{-5}$, and (d) $10^{-6} > w \geq 10^{-7}$.

Suppose that the total trajectory space is $\mathbf{C}$, which includes all possible FB paths in Hilbert space. Reduced trajectory space $\mathbf{C}_m$ can be defined such that $\mathbf{C}_m$ includes trajectories whose FB path deviation does not exceed m sites at any time, that is, $|\Delta(t)| \leq m$. The smallest trajectory space is $\mathbf{C}_0$, which consists of classically allowed paths only. Because we are dealing with a five-state Hilbert space, the maximum FB path deviation can be four so that the largest trajectory space is $\mathbf{C}_4$, which is equivalent to the total trajectory space, thus $\mathbf{C}_0 \subset \mathbf{C}_1 \subset \mathbf{C}_2 \subset \mathbf{C}_3 \subset \mathbf{C}_4 \equiv \mathbf{C}$.

In Figure 4, the average of the absolute FB path deviation, $\langle|\Delta(t)|\rangle$, is presented along with its standard deviation, $\sigma(t)$. The averages in Figure 4a were taken among trajectories that have considerably large weights as $w \geq 10^{-1}$, whereas Figure 4b−d resulted from paths with a weight as small as 10^{-7}; that is, trajectories with large FB path deviations tend to have smaller weights, as expected from eq 12. In all cases shown in Figure 4, $\langle|\Delta(t)|\rangle + \sigma(t) \leq 1$. It is visible that both the average value and the standard deviation increase for small path weights. In our tight-binding model, distance between the nearest-neighbor states was set to be equal to unit distance; thus, the results in Figure 4 indicate that the difference between the forward and backward quantum mechanical paths spans no further than the nearest-neighbor states. In terms of the reduced trajectory space, $\mathbf{C}_1$ contributes the most and the paths that do not belong to $\mathbf{C}_1$ may be ignored without causing any noticeable numerical error.

In the absence of the bath, the five-state system exhibits completely coherent dynamics because there is no quantum docoherence arising from the dissipative environment. Therefore, we performed the characteristic analysis on the bare five-state system dynamics. Without dissipation, charge population is no longer localized; it oscillates within the entire system. Figure 5 shows distinct change from Figure 4 that the average value and the standard deviation increased dramatically even for paths with large weights. The average difference between the FB path is

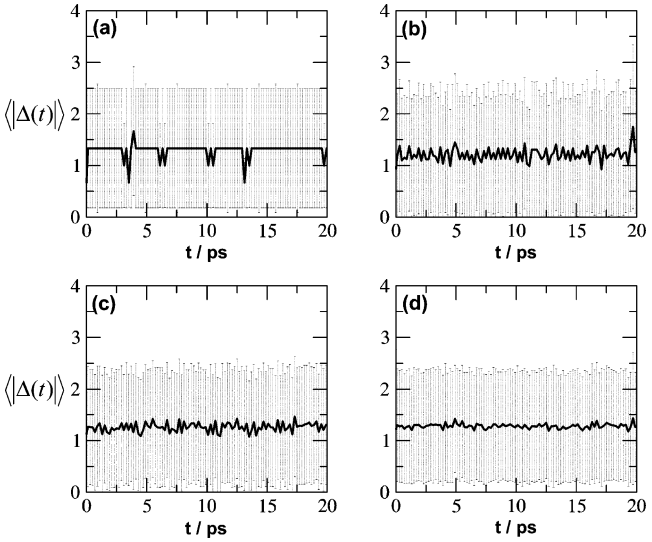

Figure 5. Same as Figure 4 in the absence of the bath.

larger than one unit distance, indicating that the FB path correlation is strong. In addition, the standard deviation is larger than one unit distance, which implies that the majority of the quantum trajectories are actively involved in the completely coherent dynamics such that, unlike the incoherent hopping transfer, the total trajectory space should have been taken into account to reproduce accurate quantum dynamics. From the two cases shown in Figures 4 and 5 along with the fact that the classical trajectories have no FB path deviation, it is clear that the quantitative value of the FB path deviation depends on the nature of the CT dynamics and the coherence within the system. Therefore, it is reasonable to consider the FB path deviation as a characteristic criterion for the CT mechanism.

To explore the quantitative effect of the FB path deviation to the density matrix, Figure 6 compares the population relaxation that are obtained by integrating paths that belong to $\mathbf{C}_k$ trajectory space by varying k from 0 to 4. Five diagonal elements of reduced density matrix and its normalization, $\sum_{i=1}^{5} \tilde{\rho}_{ii}$, are presented. In accordance with Figure 4, path integration in reduced trajectory spaces larger than $\mathbf{C}_1$ including itself produced excellently converged results. Preventing deviation between the FB path no further than the nearest neighbor obviously was sufficient to give rise to numerically accurate quantum dynamics. Although it is not presented, diagonal elements of the system density matrix in the absence of the bath converge only if all of the possible paths in the **C** trajectory space are considered and the use of any reduced trajectory space caused significant error.

We examine the influence of the FB path deviation on the off-diagonal elements, which represent quantum coherence. Figure 7a compares off-diagonal elements between nearest-neighbor diabatic surfaces, $\tilde{\rho}_{12}$, $\tilde{\rho}_{23}$, $\tilde{\rho}_{34}$, and $\tilde{\rho}_{45}$ that are obtained by integrating trajectory spaces $\mathbf{C}_1$ and $\mathbf{C}_4$, respectively. Even though the scale of the values is 2 orders of magnitude smaller than that of the diagonal elements, there is no remarkable error in the reduced trajectory space integration. On the contrary, the off-diagonal elements between distant states, such as $\tilde{\rho}_{13}$, $\tilde{\rho}_{14}$, $\tilde{\rho}_{15}$, show discrepancy in Figure 7b when we have ignored the paths with the FB path deviation larger than the unit distance. This behavior illustrates that the quantum mechanical paths with large FB path deviation participate in quantum coherence such that restricting the deviation may cause error in the off-diagonal density matrix elements. Nonetheless, the numerical errors caused by the use of the reduced trajectory space are negligible.

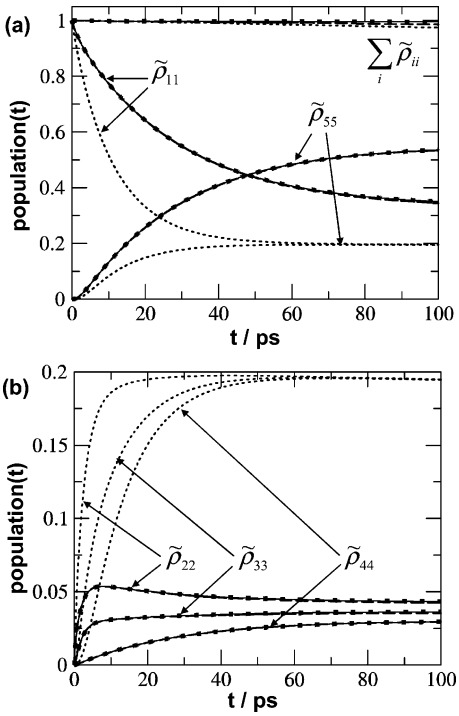

Figure 6. Five diagonal elements of reduced density matrix for the F1 configuration in Table 1; (a) donor ($\tilde{\rho}_{11}$) and acceptor ($\tilde{\rho}_{55}$) populations and (b) bridge ($\tilde{\rho}_{22}$, $\tilde{\rho}_{33}$, $\tilde{\rho}_{44}$) populations. Path integration has been performed, respectively, in $\mathbf{C}_0$ (dotted lines), $\mathbf{C}_1$ (dashed lines), $\mathbf{C}_2$ (dot−dashed lines), $\mathbf{C}_3$ (solid lines), and $\mathbf{C}_4$ (squares) reduced trajectory spaces. (For definitions of reduced trajectory space, see the text.) Although $\mathbf{C}_0$ consists of classically allowed paths only, $\mathbf{C}_4$ is equivalent to the total trajectory space. Lines near 1 are normalizations defined as the sum of diagonal elements $\sum_{i=1}^{5} \tilde{\rho}_{ii}$. For all of the simulations shown, $\theta = 10^{-8}$ was used.

B. Coherent Migration Contributed Charge Transfer. Next, we consider the F2 configuration given in Table 1 that is expected to exhibit coherent nature in transfer processes because of the high bridge energies. Potential parameters for the F2 configuration were adapted from the DNA hole transfer system such that they mimic a 5′-G(AAA)GGG-3′ double helix with three A/T bridge base pairs between a single G/C base pair donor and a triple G/C base pair acceptor. CT dynamics within the sequence has been known to have strong coherence because of the unstable redox potential of the A/T base pair for the hole transfer. For a short DNA sequence like 5′-G(A)GGG-3′, superexchange migrations between donor and acceptor readily occur. However, the superexchange contribution is expected to decrease dramatically with the bridge length, because of the exponential decay of the superexchange coupling constants. In Figure 8, five diagonal density matrix elements obtained by the full path integration and by the incoherent hopping pathway integration show great discrepancies, indicating that the overall transfer is governed not by a single mechanism but by the interplay between the incoherent and partially coherent hopping mechanisms. Although incoherent migrations play an important role during the initial CT, contribution from the coherent transfer becomes dominant over time.

In Figure 9, FB paths relevant to the CT dynamics of the F2 configuration are analyzed and presented. It is seen that the average difference between FB paths is larger than that observed in Figure 4 for the incoherent hopping-dominated case. The average difference is approximately one, that is, nearest-neighbor states, and the standard deviation extends the FB path deviation to the next-nearest-neighbor states. Without decoherence introduced by a thermal bath, in Figure 10, the FB path deviation of

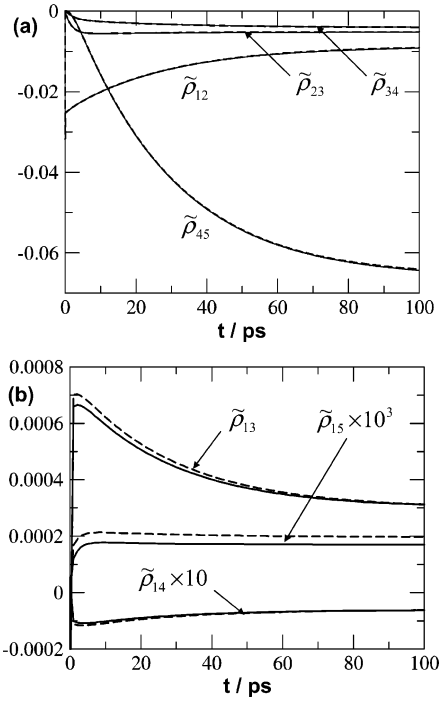

Figure 7. Off-diagonal elements of the reduced density matrix of the F1 configuration in Table 1. Although solid lines are obtained using the OFPF-PI method on the total trajectory space **C**, dashed lines are resulted from integrating paths in $\mathbf{C}_1$ reduced trajectory space. (a) $\tilde{\rho}_{12}$, $\tilde{\rho}_{23}$, $\tilde{\rho}_{34}$, and $\tilde{\rho}_{45}$ and (b) $\tilde{\rho}_{13}$, $\tilde{\rho}_{14}$, and $\tilde{\rho}_{15}$. For all of the simulations shown, $\theta = 10^{-8}$ was used.

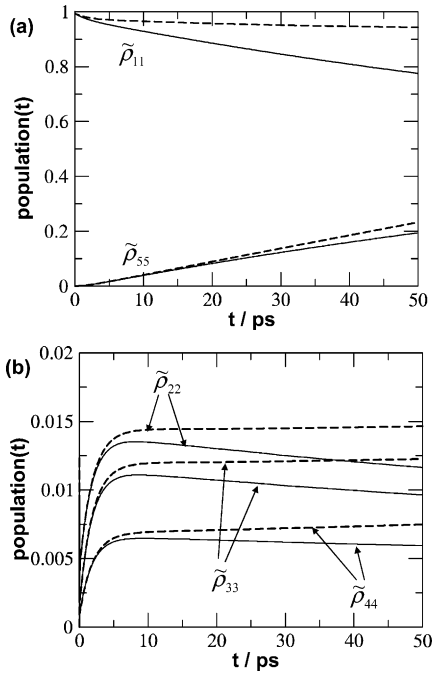

Figure 8. Same as Figure 3 for the F2 configuration in Table 1.

the bare F2 system is even greater. Particularly, for the paths with weights as small as $10^{-7} \leq w < 10^{-6}$ in Figure 10d, the forward path and backward path differ by two states on average. In addition, the standard deviation indicates that the whole system exhibits very strong coherence in dynamics. By comparing Figures 5 and 10, even in the absence of the bath, the F2 bare system inherently has more coherent nature than the F1 bare system. For both cases, it was obviously expected that the bath has decreased coherence within the system through dissipative interference.

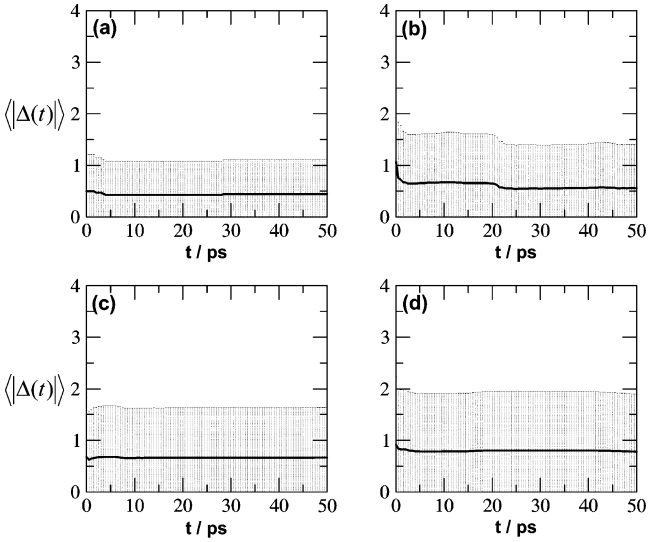

Figure 9. Same as Figure 4 for the F2 configuration in Table 1.

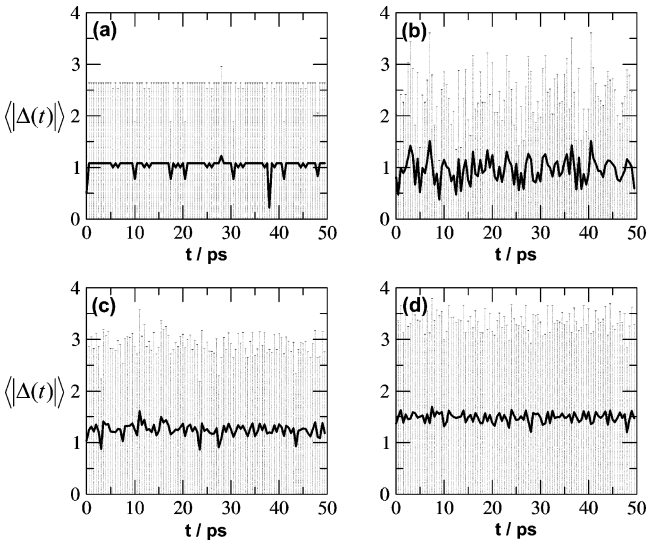

Figure 10. Same as Figure 5 for the F2 configuration in Table 1.

Quantitative comparison of the reduced trajectory space path integration in Figure 11 agrees well with the analysis on the FB path deviation shown in Figure 10. According to Figure 11, one should at least consider the $\mathbf{C}_2$ trajectory space in order to obtain converged diagonal density matrix elements. Nevertheless, relative contribution of the incoherent hopping mechanism to the CT processes within the F2 configuration is still significant so that integrating paths that belong to the $\mathbf{C}_1$ trajectory space produced qualitatively reasonable results. $\mathbf{C}_2$ trajectory space integration gives rise to accurate numerical results for the off-diagonal density matrix elements between nearest diabatic surfaces such as $\tilde{\rho}_{23}$: however, error is accumulated for those between distant diabatic surface such as $\tilde{\rho}_{24}$ and $\tilde{\rho}_{25}$ as depicted in Figure 12. Although the absolute magnitude is small, correlation within the bridge states, which are represented by the magnitude of the corresponding off-diagonal density matrix elements, is substantially stronger compared to that of the bridge-acceptor states. It is also interesting that the magnitude of $\tilde{\rho}_{24}$ is in fact twice as large as that of $\tilde{\rho}_{23}$ despite the distance. As observed in quantum mechanical tunneling phenomena, it illustrates that the quantum dynamical characteristics of coherence are irrelevant to the distance unlike the classical counterpart.

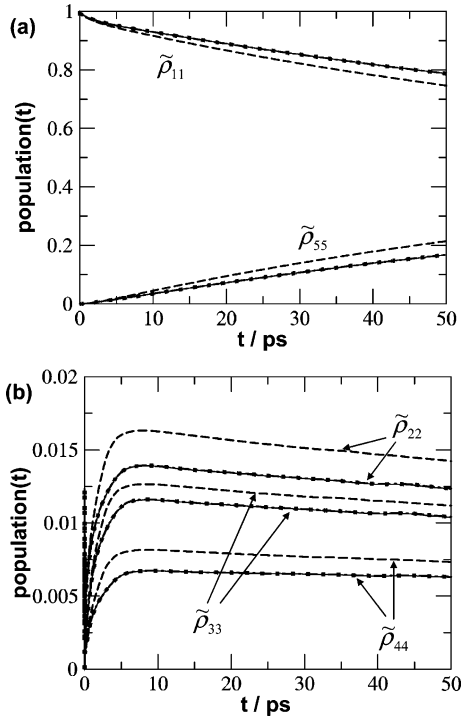

Figure 11. Five diagonal elements of reduced density matrix for the F2 configuration in Table 1; (a) donor ($\tilde{\rho}_{11}$) and acceptor ($\tilde{\rho}_{55}$) populations and (b) bridge ($\tilde{\rho}_{22}$, $\tilde{\rho}_{33}$, $\tilde{\rho}_{44}$) populations. Path integration has been performed, respectively, in $\mathbf{C}_1$ (dashed lines), $\mathbf{C}_2$ (dot−dashed lines), $\mathbf{C}_3$ (solid lines), and $\mathbf{C}_4$ (squares) reduced trajectory spaces.

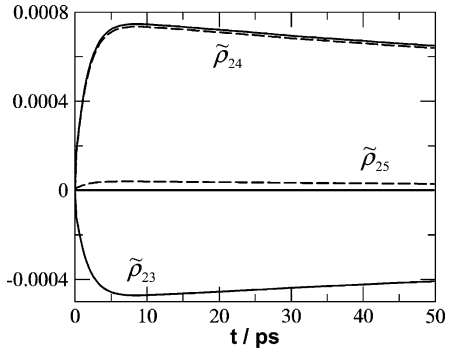

Figure 12. Off-diagonal elements of the reduced density matrix of the F2 configuration in Table 1. Although solid lines are obtained using the OFPF-PI method on the total trajectory space **C**, dashed lines are resulted from integrating paths in $\mathbf{C}_2$ reduced trajectory space. $\tilde{\rho}_{23}$, $\tilde{\rho}_{24}$, and $\tilde{\rho}_{25}$ are shown.

4. Concluding Remarks

One of the major limitations of the current multistate quantum mechanical simulations is the exponential scale of the computation with respect to the system size and propagation time. However, it has been known that the vast majority of the quantum mechanically allowed paths make insignificant contributions to the actual dynamics, particularly to the dynamics in the condensed phase. Therefore, an optimized way of searching quantum dynamically meaningful paths is vital for efficient simulations of large systems. In this article, we examined characteristics of the quantum mechanically important paths that have been selected through on-the-fly filtering processes of the OFPF-PI method and showed that the difference between the FB paths depends strongly on the type of dynamics. The deviation is large for coherent systems and decreases as the system dynamics approaches the incoherent limit. It may be obvious that the incoherent hopping dynamics is governed by the classical analogues, that is, FB paths with little deviation. However, as far as we know, there has been no quantitative analysis on quantum mechanical pathways, particularly on FB pathways to the CT dynamics. This article, for the first time, presented the quantitative analysis on the quantum dynamically significant pathways and introduced a practical simulation algorithm for the long-range incoherent hopping-dominated molecular wire systems.

As discussed in this article, for the case of the five-state incoherent hopping-dominated CT dynamics, the FB path deviation expands only to the nearest neighbors. The argument applies regardless of the search algorithm whether it is based on the statistical techniques or it mimics exact integration utilizing a smart algorithm such as the on-the-fly filtering scheme. It illustrates that, as one performs the path integration on the multistate Hilbert space, it is possible to consider only a fraction of the trajectory space guided by the predetermined characteristics of the paths without wasting computation resources that take to sample all trajectories. In addition, although we used a harmonic oscillator bath, the path characteristics are also applicable to anharmonic baths, in which the influence functional may be treated perturbatively.[24] On the basis of that, we suggest a rigorous exact integration method that takes advantage of *a priori* information of the quantum mechanical paths. Incoherent hopping-dominated long-range CT system may be the most benefited by considering only the nearest-neighbor transitions. For the coherent migration-dominated processes, the FB path deviation can be significant depending on the coherence of the system. Formulation of the relationship between the FB path deviation and the coherence is currently in progress and will be explored in future publications.

Acknowledgment. This work was supported by the Korea Research Foundation Grant funded by the Korean Government-(MOEHRD) (KRF-2005-015-C00204) in which main calculations were performed by using the supercomputing resource of the Korea Institute of Science and Technology Information (KISTI). We also acknowledge the Molecular Science Research Institute at Yonsei University.

References and Notes

(1) Miller, W. H. *Proc. Natl. Acad. Sci.* **2005**, *102*, 6660 and references therein.
(2) Feynman, R. P.; Vernon, F. L. *Ann. Phys.* **1963**, *24*, 118.
(3) Feynman, R. P.; Hibbs, A. R. *Quantum Mechanics and Path Integrals*; McGraw-Hill: New York, 1965.
(4) Salieres, P.; Carre, B.; Le Deroff, L.; Grasbon, F.; Paulus, G. G.; Walther, H.; Kopold, R.; Becker, W.; Milosevic, D. B.; Sanpera, A.; Lewenstein, M. *Science* **2001**, *292*, 902.
(5) Poulsen, J. A.; Nyman, G.; Rossky, P. J. *J. Phys. Chem. B* **2004**, *108*, 19799.
(6) Mikami, T.; Okazaki, S. *J. Chem. Phys.* **2004**, *121*, 10052.
(7) Mühlbacher, L.; Ankerhold, J. *J. Chem. Phys.* **2005**, *122*, 184715.
(8) Sim, E. *J. Phys. Chem. B* **2005**, *109*, 11829.
(9) Davis, W. B.; Wasielewski, M. R.; Ratner, M. A.; Mujica, V.; Nitzan, A. *J. Phys. Chem. A* **1997**, *101*, 6158 and references therein.
(10) McConnell, H. M. *J. Chem. Phys.* **1961**, *35*, 508.
(11) *Quantum Monte Carlo Methods in Condensed Matter Physics*; Suzuki, M., Ed.; World Scientific: Singapore, 1993 and references therein.
(12) Egger, R.; Mak, C. H. *Phys. Rev. B* **1994**, *50*, 15210.
(13) Egger, R.; Mak, C. H. *J. Phys. Chem.* **1994**, *98*, 9903.
(14) Makri, N.; Makarov, D. E. *J. Chem. Phys.* **1995**, *102*, 4600.
(15) Makri, N.; Makarov, D. E. *J. Chem. Phys.* **1995**, *102*, 4611.
(16) Sim, E.; Makri, N. *Chem. Phys. Lett.* **1996**, *249*, 224.
(17) Sim, E.; Makri, N. *Comput. Phys. Commun.* **1997**, *99*, 335.
(18) Sim, E. *J. Chem. Phys.* **2001**, *115*, 4450.
(19) Sim, E. *J. Phys. Chem. B* **2004**, *108*, 19093.
(20) Sim, E.; Makri, N. *J. Chem. Phys.* **1995**, *102*, 5616.
(21) May, V.; Kühn, O. *Charge and Energy Transfer Dynamics in Molecular Systems*; Wiley−VCH: Weinheim, 2004.
(22) Giese, B.; Amaudrut, J.; Köhler, A.-K.; Spormann, M.; Wessely, S. *Nature* **2001**, *412*, 318.
(23) Imparato, A.; Peliti, L. *Phys. Rev. E.* **2005**, *72*, 046114.
(24) Makri, N. *J. Phys. Chem.* **1999**, *103*, 2823.